Carbon 178 (2021) 657–665

Contents lists available at ScienceDirect

Carbon

journal homepage: www.elsevier.com/locate/carbon

Research Article

In-situ growth of single-crystal plasmonic aluminum–lithium-graphene nanosheets with a hexagonal platelet-like morphology using ball-milling

Sara I. Ahmad [a, *], Hicham Hamoudi [b], Janarthanan Ponraj [b], Khaled M. Youssef [c]

[a] Department of Sustainable Development, Hamad Bin Khalifa University, Doha 5825, Qatar
[b] Qatar Environment and Energy Research Institute, Doha 34110, Qatar
[c] Department of Materials Science and Technology, Qatar University, Doha 2713, Qatar

ARTICLE INFO

Article history:
Received 9 January 2021
Received in revised form
25 March 2021
Accepted 26 March 2021
Available online 31 March 2021

Keywords:
Single-crystal
Plasmonic
Graphene
Aluminum
Hexagonal nanoplatelets
Ball-milling

ABSTRACT

Metal-graphene nanocomposites and plasmonic metal nanoparticles are two nanoscience fields of a rapidly growing interest due to their potential in advanced applications. In this study, we combine both fields by synthesizing plasmonic aluminum-lithium-graphene nanosheets (Al–Li-GNSs) with anisotropic morphologies using a simple ball-milling technique. Structural analysis using SEM and TEM revealed that the Al–Li-GNSs nanoparticles are single-crystals with a hexagonal platelet-like morphology of a ~300 –500 nm diagonal and a ~60 nm thickness. Electron diffraction analysis indicated that the as-milled platelets have an FCC structure with (111) top and bottom facets and revealed the presence of 1/3(422) and 1/3(220) forbidden reflections. UV–Vis spectroscopy of the hexagonal Al-based nanoplatelets was found to exhibit plasmonic resonance absorption bands in the UV region at a wavelength of 214 nm and 345 nm. In this report, we confirm the feasibility of building epitaxial plasmonic metal-graphene systems inside bulk metal-graphene composites using a simple milling process.

1. Introduction

The synthesis and development of noble metal nanoparticles lays at the core of nanotechnology and is a landmark in the history of modern nanoscience [1]. The unique localized surface plasmon resonance of metallic nanoparticles has shown tremendous potential for cutting-edge applications such as photocatalysis [2,3] and sensing [4,5]. Recent advancements in the synthesis of aluminum (Al) nanoparticles with controlled sizes and anisotropic shapes rendered the utilization of Al as a practical alternative to the more famous noble metal nanoparticles [6,7]. Its high energy density and high enthalpy of combustion ranked Al nanoparticles as a promising material in propellants and explosives [8,9], and a thriving component for hydrogen production [10,11], and energy storage [12,13]. The electronic structure of Al allows it to sustain a more flexible optical performance than that of coinage metals (Cu, Au, or Ag), supporting a larger range of wavelengths extending over the entire UV–Vis-IR spectrum [6,14,15].

Despite the recent interest in Al nanoparticles, the advancement in its synthesis is far behind that of noble metals such as Au and Ag [16] due to its higher reactivity [7,17]. Today, refined protocols of the Haber's method [18] remain the most commonly used technique to produce Al nanoparticles [6,7,19], with recent advances reported using electric arc-discharge [20], lithography [21], or laser ablation [22]. Nonetheless, a simple, cost-effective, nonchemical-based synthesis technique is yet to be reported, hindering large-scale production of Al nanoparticles.

On another front, scientists have been actively investigating the possibility of using the 2D graphene substrate to grow metallic nanoparticles. While several experimental and computational investigations have been reported, the synthesis of 2D metal/graphene systems is hindered by the little understanding achieved thus far of the metal/graphene interfacial atomic interactions [23,24]. Efforts in reinforcing 3D bulk metal matrices with graphene nanosheets (GNSs), however, have been reported using a wide range of techniques, and the macroscopic properties of such composites are readily measured and characterized [25]. Mechanical, tribological, and electrical properties enhancements have been reported in graphene reinforced metal matrices [26–28]. Ball-milling has been the most widely used technique for the efficient

* Corresponding author. Tel.: +974 66633557.
E-mail address: sahmed@hbku.edu.qa (S.I. Ahmad).

https://doi.org/10.1016/j.carbon.2021.03.053

mixing and distribution of GNSs in metals as the high shear force exerted during milling results in the exfoliation of the GNSs, while the high rotation energy results in the uniform distribution of the GNSs within the Al matrix [28–30].

In this study, we report a new one-step simple dry ball-milling synthesis of single-crystal Al–Li-GNSs nanoparticles with hexagonal platelet-like morphologies that exhibit high plasmonic absorbance. In this regard, we confirm the feasibility of building epitaxial metal-graphene systems inside bulk metal-graphene composites using a simple milling process.

2. Materials and methods

2.1. Materials and synthesis of anisotropic Al–Li-GNSs nanoplatelets

Pure Al powder (99.97% - Alfa Aesar) was ball milled with pure (99%) Li granules and GNSs (Sigma-Aldrich). The morphologies of the as-received Al powder with an average particle size of 15 μm and the as-received GNSs are shown in Fig. 1a and b, respectively.

The selection of the GNSs content was based on literature data, which reported an optimum content with the addition of 1.0 wt% GNSs in Al composites [31–33]. Only 0.5 wt% Li were added in order to help activate the deformation twinning in Al and to be maintained within the solid solubility of Li in Al [34,35]. The Al, Li, and GNSs were loaded into a steel vial with steel balls using a ball-to-powder ratio of 17:1 and milled using a SPEX 8000 shaker mill for 8 h at room temperature. The milling was stopped every hour, and the vial was placed in a freezer (−18 °C) for 10 min to cool the vial, which helps to prevent Al welding. The loading, sealing, and handling of the sample was done in a glovebox under ultra-high purity argon (oxygen level < 0.5 ppm) to eliminate oxidation during milling.

2.2. Characterization of as-milled anisotropic Al–Li-GNSs nanoplatelets

Structural and morphological analysis of the as-milled Al–Li-GNSs nanoplatelets was carried out using scanning electron microscopy (SEM) and transmission electron microscopy (TEM). The SEM images of the as-milled nanoplatelets were acquired using a FEI Nova NanoSEM 450 operated at an accelerating voltage of 5 kV and a working distance of 5 mm. The TEM analysis was performed using a Thermo Scientific TalosF200X TEM and a FEI TECNAI G^2 FEG TEM, both operating at 200 keV to obtain bright-field and STEM-HAADF images, as well as the selected area electron diffraction (SAED) of the as-milled nanoplatelets. The TEM samples were prepared by sonicating the as-milled powder in isopropyl alcohol for 10 min. A 20 μl of the dispersed solution was dropped over a 300 mesh carbon grid and then dried at room temperature. X-ray diffraction (XRD) spectrum of the as-milled nanoplatelets was collected using a PANalytical Empyrean Diffractometer with a CuK_α ($\lambda = 0.1542$ nm) radiation. The XRD operating conditions were carried out at 45 kV, 40 mA, and 25 °C with scanning range from 20° to 100°, a step size of 0.013°, and a scan rate of 0.044° s^{-1}. A Thermo fisher scientific DXR Raman spectroscopy with a laser wavelength of 532 nm was used to examine the structural integrity of the GNSs after milling. Optical absorption spectra of the as-milled powders were recorded using a SHIMADZU UV-2600i UV–Vis spectrophotometer in a double beam mode with a scanning range of 200–900 nm. The optical colloid was prepared by sonicating the as-milled powder in ethanol for 30 min before analysis. The colloid was left to settle, and then it was filtered to remove the larger-sized particles before testing.

3. Results

The morphology of the as-milled Al–Li-GNSs particles was first examined by SEM, see Fig. 2. Typically, the ball-milling of Al powders yields round-shaped particles, which agglomerate together to form flat flakes [30,36] or hollow spheres with prolonged milling times [37]. This is a result of the high impact and shear forces exerted by the steel balls and the vial's walls, causing the continuous deformation of Al [36]. However, particles with a perfect hexagonal platelet-like morphology and well-defined facets appear to be distributed throughout the Al–Li-GNSs as-milled sample, see Fig. 2a–b. The diagonal of the hexagonal platelets varies from 260 nm to 580 nm, while the thickness is measured to be around 60 nm, as could be distinguished from the SEM image in Fig. 2b. The GNSs were not detected by SEM due to their low content and small dimensions. During milling, the GNSs are homogeneously distributed in the Al matrix due to the high shear-force of the milling process. Moreover, the GNSs are expected to be embedded in the Al matrix due to the ductility of Al, which leads to sandwiching the graphene sheets in between the Al particles [29,38].

This well-defined morphology is an indirect evidence of the crystallinity of the nanoplatelets, where such structures are reported to be a result of a single-crystal growth with a preferred

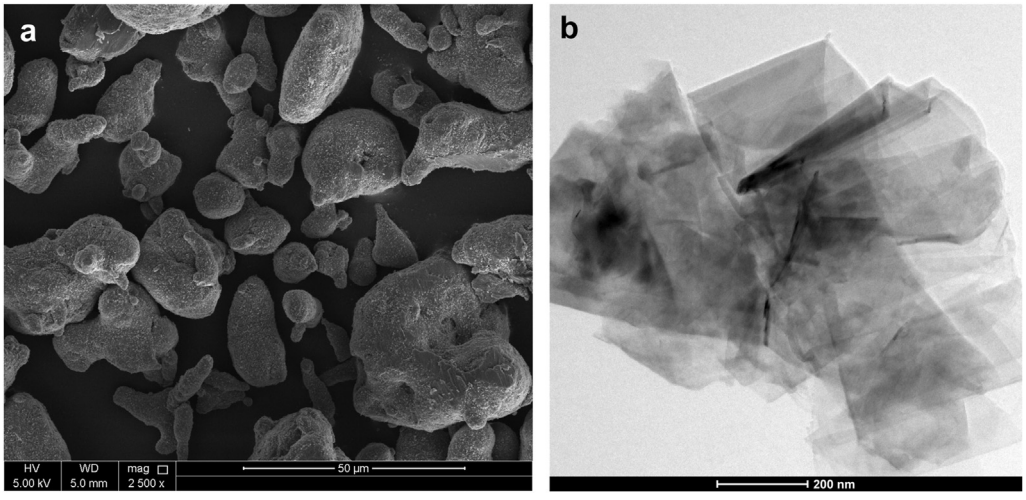

Fig. 1. a) An SEM image of the gas-atomized as-received Al particles, b) A bright-field TEM image of the as-received GNSs.

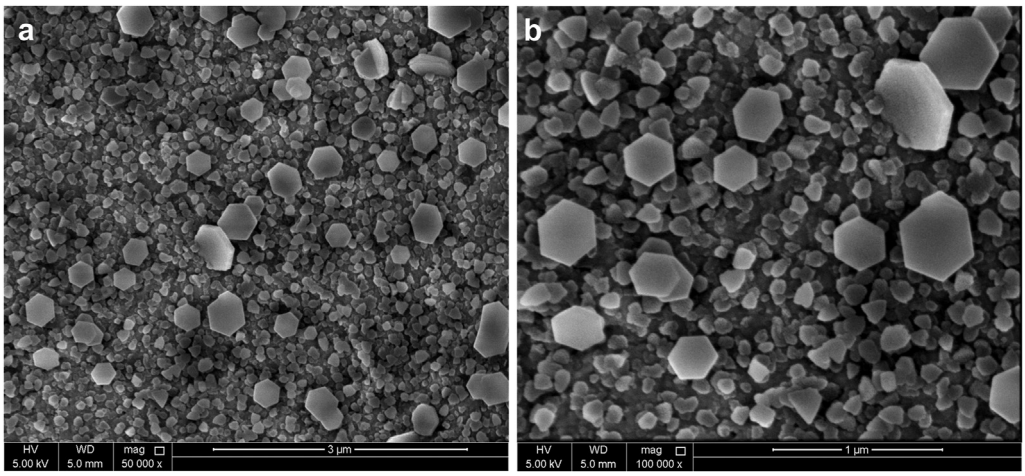

Fig. 2. a) SEM image of the as-milled Al–Li-GNSs milled for 8 h, and b) magnification of a). The images show a clear formation of hexagonal nanoplatelets after milling.

orientation [39]. Similar hexagonal and triangular platelet structures have been frequently reported for noble metals such as Ag and Au via colloidal-based chemical synthesis techniques [39–43]. Recently, the synthesis of Al nanoparticles with controlled morphologies such as single-crystal Al nanocubes [6], nanorods [44], Nanoantennas [21], nanodisks [14] triangular prisms [15] trigonal bipyramids [45], and octahedron nanoparticles [46], have also been reported.

Phase investigations of the as-milled sample were conducted by XRD. The XRD pattern of the Al–Li-GNSs nanoplatelets showed only a face-centered cubic (FCC) Al phase, see Fig. 3a. No peaks were observed for the body-centered cubic (BCC) Li or any Al–Li second phases in the XRD pattern. This is attributed to the complete solubility of Li in Al, resulting in the formation of an FCC solid solution. It is well-established experimentally that ball-milling can increase the solid solubility limit beyond the conventional limit, creating super-saturated solid solutions or even alloying systems from immiscible elements which otherwise do not attain an equilibrium room temperature solubility [47–49]. This is a result of the large excess segregation sites introduced in the Al lattice by ball-milling as a result of the large grain boundary density in nanocrystalline materials [50]. The absence of any peaks for the GNSs could be attributed to the low content of GNSs (1.0 wt%) used [51]. The existence of GNSs in the Al–Li matrix and the effect of milling on the structural integrity of graphene were investigated using Raman spectroscopy, see Fig. 3b. The Raman spectra of both the pure GNSs and the GNSs in the as milled Al–Li-GNSs nanoplatelets illustrate the characteristic graphene peaks at around 1350, 1580, and 2700 cm^{-1}, corresponding to the D, G, and 2D bands, respectively [52]. The G-band is associated with the in-plane C–C vibrations in a graphite lattice, the D-band is associated with sp3 lattice disorders, and the 2D-band is sensitive to the aromatic carbon structure [52]. The introduction of structural defects in the GNSs after milling is inevitable due to the intensive nature of the high energy ball-milling technique. This explains the increase in the intensity of the D-band and the intensity ratio of the D-band to the G-band (I_D/I_G) of the GNSs after milling as compared to those of pure GNSs. Lattice defects interrupt the two-dimensional translational symmetry in the graphene sheet. Thus, the D-band intensity increases and broadens with increasing number of defects [52]. After milling of the Al–Li-GNSs, the intensity of the GNSs 2D-band decreases with a significant peak broadening, see Fig. 3b. The increase in the I_D/I_G ratio from 0.14 to 1.1 is in agreement with previously reported Raman analysis for GNS-Al composites synthesized by ball-milling [25]. A positive shift in the G-band is observed after milling, which is usually attributed to the accumulated stresses in the graphene lattice caused by milling and upon binding to Al [53] and the change in the interatomic distances in the graphene after milling. Thus, the vibration frequency of the G-band changes and results in a wavenumber shift [54]. Nonetheless, the presence of a sharp G-band and the detection of a 2D-band after 8 h of milling is an indication of a preserved graphitic structure of the GNSs [52]. This could be attributed to the C–C bond strength in graphene and the ductility of Al, which helps to protect the embedded GNSs against further collision. Another graphitic lattice-defect associated band appearing after milling with a weaker intensity is the D + G band detected at around 2900 cm^{-1} in the as-milled sample [55].

The synthesis of Al nanoplatelets was also confirmed by the UV–Visible spectra of the as-milled Al–Li-GNSs sonicated in ethanol. Metallic nanoparticles exhibit a special optical behavior that is associated with specific optical resonant frequencies generated due to the interaction between the metal's electron cloud and the electromagnetic wave [56]. The UV–Vis spectrum of the hexagonal Al–Li-GNSs in Fig. 3c shows absorbance bands in the UV region below the visible range. A sharp and narrow absorbance peak can be seen at 214 nm with a shoulder at 240 nm, and a smaller broad peak at 345 nm. Plasmonic absorbance bands in the UV region are in agreement with expected and reported UV–Vis characteristic absorbance spectra of other plasmonic Al nanoparticles [6,14,15]. In addition, the sharp UV absorbance peak in Fig. 3c is an indication of the purity of the nanoplatelets [14]. These results confirm the plasmonic nature of these Al–Li-GNSs nanoplatelets synthesized by ball-milling.

Bright-field TEM images of the Al–Li-GNSs hexagonal nanoplatelets are presented in Fig. 4. An interesting TEM image showing one single-crystal hexagonal Al–Li-GNS platelet trapped in what appears to be a large, crumbled, and folded GNSs can be seen Fig. 4a–b. The structure of the hexagonal nanoplatelets appears to be symmetrical with sharp defined edges and corners, with a diagonal length of 482 nm, see Fig. 4c. The presence of sharp features in the morphology of metallic nanoparticles, such as the sharp tips in nano-octopods [6] and nano-cones [57], and the sharp corners in nano-cubes [6], is advantageous as it is reported to significantly strengthen the local plasmonic electromagnetic field and absorption cross-sections. Thus, the sharp and narrow absorption plasmon resonance peak in Fig. 3c can also be attributed to the defined edges

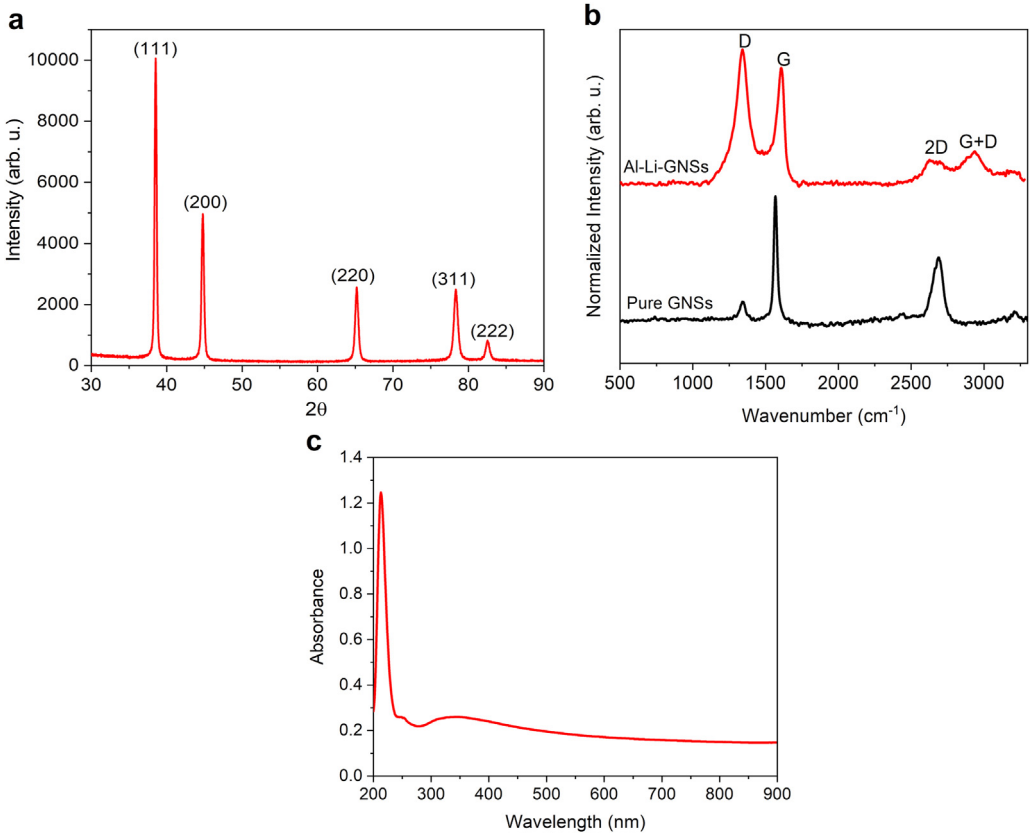

Fig. 3. a) XRD of as-milled Al–Li-GNSs nanoplatelets, b) Raman spectroscopy of the as-received GNSs and the as-milled Al–Li-GNSs, c) UV–Vis absorbance spectrum of the as-milled Al–Li-GNSs dispersed in ethanol. (A colour version of this figure can be viewed online.)

and sharp corners of the hexagonal Al–Li-GNSs nanoplatelet, as can be seen in Fig. 4c. This is attributed to the ability of sharp structural features such as corners and tips to concentrate incident light due to the lightning rod effect and reduced radiative damping, causing more light to be absorbed and resulting in stronger UV absorbance bands, as shown in Fig. 3c [56].

The spot pattern of the corresponding SAED pattern taken perpendicular to the flat top facet of the hexagon is shown in Fig. 4d, and it confirms the single-crystallinity of the hexagonal nanoplatelet. Diffraction spots with d-spacings of 0.143 nm and 0.0826 nm can be assigned to the Al (220) and (422) atomic planes, respectively. The d-spacing measurements and the 6-fold symmetry of the SAED indicate that the flat top and bottom facets of the hexagons are (111) Al atomic planes. In addition, the other two sets of spots with 6-fold symmetry and larger d-spacings of 0.429 nm and 0.248 nm are identified in the SAED in Fig. 4d. These spots match the forbidden reflections from the 1/3(220) and 1/3(422) atomic planes, respectively. Forbidden reflections from the 1/3(422) atomic planes have been reported in single-crystal flat and thin platelet-like FCC structures such as Au and Ag [39,40,42]. Several structural interpretations of the presence of these reflections have been reported [58]. The common thread is the presence of stacking faults and/or twinning planes parallel to the (111) flat facets [40], both of which break the normal systematic sequence of the FCC structure [59], leading to the 2D nucleation and growth and the formation of anisotropic well-defined structures [60]. The broken symmetry in thin FCC platelets induced by the presence of stacking faults and twinning planes is reflected in the SAED patterns as additional spots, which otherwise, are considered forbidden in the FCC structure.

Despite the emerging number of studies reporting the formation of Al single-crystal nanoparticles with anisotropic morphologies, their corresponding electron diffraction patterns are rarely reported. Thus, it is reasonable to assume that the 1/3(422) forbidden reflections have not been reported or observed before for Al-based nanoparticles. This could be related to the lack of reports on the synthesis of hexagonal 2D platelet-like Al structures, for which the forbidden reflections seem to be a pre-requisite associated with their formation. To the best of our knowledge, the 1/3(220) forbidden reflections were not observed or reported earlier for any FCC metallic nanoparticle. HAADF-STEM images of a hexagon Al–Li-GNS single-crystal nanoplatelet and its corresponding elemental mappings are presented in Fig. 5a–c. The mapping shows the homogenous distribution of both C and Al inside the single-crystals. The density of the Al atoms appears to be higher inside the hexagon, while the C atoms appear to be situated more around the boundaries and the edges of the platelet. The TEM images in Figs. 4 and 5 confirm the coexistence and interaction between the Al and the GNSs.

Another interesting feature observed in several TEM images is the presence of a triangle-like region in the middle of the individual hexagons, see Figs. 4c and 5a. These triangular areas are darker and thus thicker than the edge regions of the hexagonal nanoplatelets. Their presence could indicate that the nucleation of these hexagonal nanoplatelets starts from the middle of the hexagon on a (111) triangular facet, which later grows into a full hexagon. Another explanation would suggest that at a certain thickness, redirected growth from a hexagonal platelet to a triangular one takes place. The interplay and shape transformation between triangular and hexagonal morphologies have been reported and verified experimentally for FCC metallic nanoplatelets [41,61].

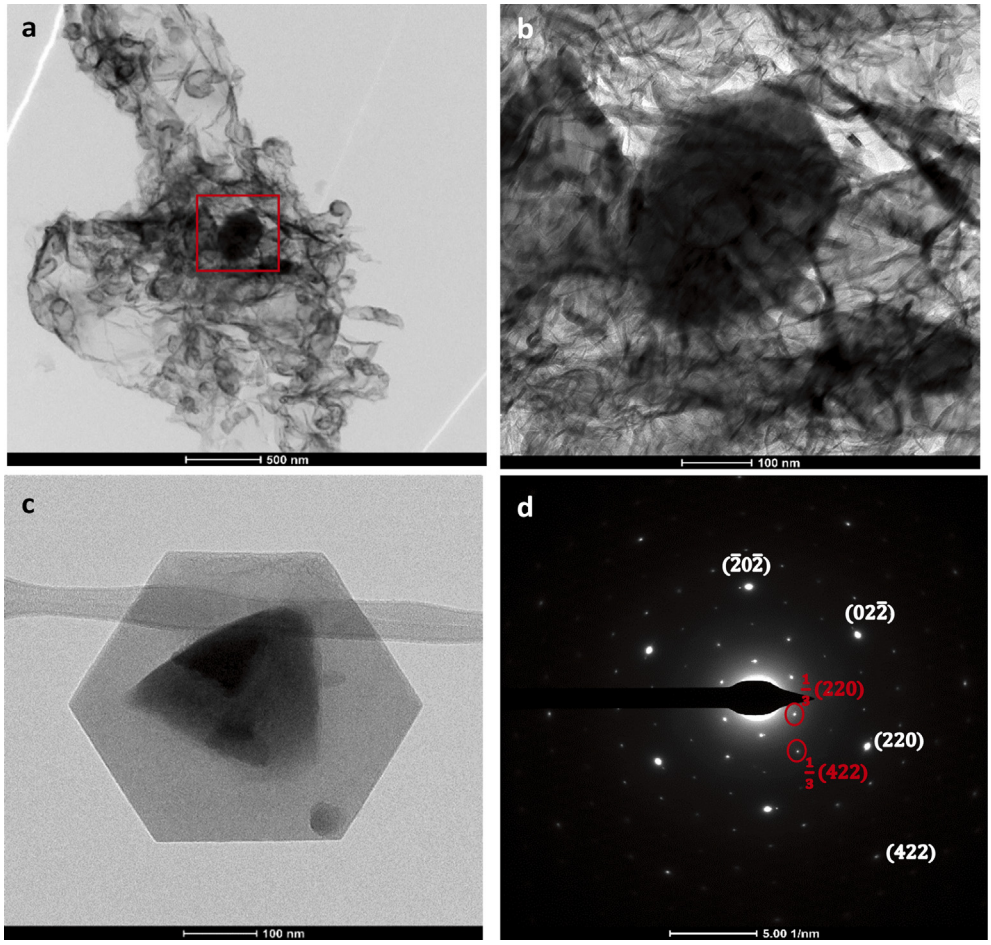

Fig. 4. a) BF-TEM image of a single-crystal Al–Li-GNSs hexagonal platelet trapped in graphene, b) magnification of red box in a), c) BF-TEM images of an Al–Li-GNSs hexagonal platelet, and d) SAED of c) in the <111> zone axis. (A colour version of this figure can be viewed online.)

4. Discussion

Both ball-milling of Al powder [28,30,62] and colloidal chemical synthesis of Al nanoparticles [44–46] have been investigated and reported by various research groups. Yet the synthesis of anisotropic hexagonal Al nanoplatelets has not been reported before. Furthermore, and to the best of our knowledge, the synthesis of anisotropic nanoplatelets of any system using ball-milling has not been reported either. In this study, we believe that the formation of well-defined single-crystal Al–Li-GNSs nanoplatelets is a result of both the utilized ball-milling system and the milled system components (the addition of both Li and GNSs).

It is well-known that ball-milling is a sensitive technique to the varying milling parameters involved in the milling process. This includes the milling energy, milling time, milling temperature, and other milling dynamics such as the ball to powder ratio, the number and size of milling balls, and the presence of process control agents (PCAs) [63]. This explains why different research groups investigating the milling of the same components observed and reported different results in terms of microstructure, grain size, deformation mechanisms, properties, and performance [64]. It is a general practice for most researchers to use PCAs during milling of ductile materials such as Al in order to prevent welding [32,65,66]. In this study, no process control agents or surfactants were used. The presence of the GNSs and its self-lubricating nature that stems from the weak van der Waals attraction forces between the graphene sheets could allow sliding of the sheets in between the Al particles during milling, thus acting as a PCA. When a PCA is used during milling, the PCA forms a layer on the Al powder covering its surface to prevent its welding. In our study, the absence of any PCAs during the milling of Al and GNSs enables a direct physical interaction between the two components, which enhanced the adhesion between the Al and the GNSs and allowed for an interfacial relationship between the two components of the system.

At this stage, one question lingers: Is there a link between the presence of graphene and the hexagonal platelet-like formation? It is unrealistic to ignore the presence of graphene and its possible influence as a 2D hexagonal substrate on the formation and growth of these 2D hexagonal platelet-like particles. Single-crystal formation requires a nucleus, a template, or a substrate on which the single-crystal growth is initiated and directed. Different metals with different structures tend to crystalize along different directions on 2D substrates such as graphene [67]. This is attributed to the tendency of the system to reduce the lattice misfit between the metal and the graphene sheet, and thus relax the excess stress at the interface [68]. During milling, the ductile Al particles are flattened, while the GNSs are sandwiched between the flat Al particles. The initial incompatibility of the Al and the graphene lattices, along with the defected sites induced by milling on both the GNSs and Al, generate excess stresses at their interfaces. As a result, the Al atoms diffuse and rearrange to achieve the most energetically favorable structure. In other words, this provides the driving force for the system to achieve a more equilibrium structure by seeking an atomic configuration that will allow for the lowest

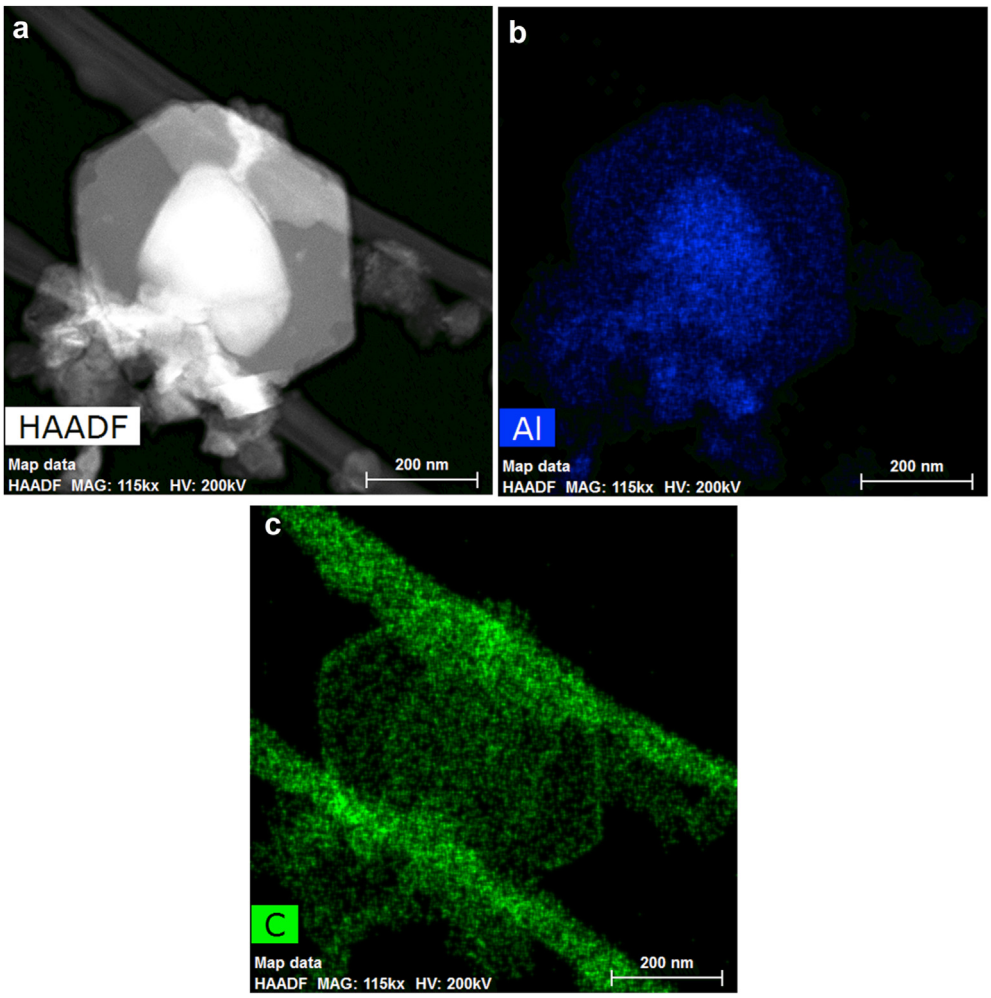

Fig. 5. a) HAADF image of a hexagonal Al–Li-GNSs nanoplatelet, b-c) elemental mapping of a). (A colour version of this figure can be viewed online.)

energy possible, and creates the conditions for a preferred (111)/(0002) Al/graphene interfacial interaction. This is supported by computational studies which showed that the Al atoms arrange in the (111) facet of the FCC structure at the Al/graphene interface [68,69] to reduce the lattice misfit. This simulation finding has been proven experimentally for other FCC metals grown on graphene, such as Pb and Au [24]. In addition, recent MDS studies revealed that solid-phase structural relaxation between Al and graphene could occur even at room temperature [68].

The graphene sheets' tendency to diffuse into the boundaries of nanostructures has also been reported theoretically [68] and experimentally [25]. This explains why the C atoms concentration is higher around the edges of the single-crystal platelet, as seen in the mapping in Fig. 5, and is attributed to the graphene sheets' tendency to further reduce the lattice misfit and achieve a stable structure [68]. One can also consider that the graphene sheets are defining the shape of the hexagonal single-crystals and that the flat crystals are laterally limited by the GNSs inside the platelets. This suggestion requires further investigations to validate the role of the graphene sheets around the boundaries of the single-crystals. Based on these observations, we conclude that the graphene sheets distributed inside the hexagon platelet are providing the interface with the Al on which the anisotropic growth is initiated, while excess graphene sheets mitigate through the lattice and reside on the boundaries to further reduce the lattice misfit and achieve a more stable structure.

The growth of the hexagonal nanoplatelets is then supported by the context of the Gibbs-Wulff theorem, and induced by the presence of Li. The anisotropy of the surface energy of crystalline solids suggests that the total surface energy is not only determined by the surface area, but by the type of the enclosed surface facets as well. For an FCC nanoparticle, maximizing the expression of the (111) facets in the structure results in minimizing the total surface energy [70], leading to the formation of a truncated tetrahedral or octahedral shapes enclosed by (111) facets [71]. The SAED pattern in Fig. 4d taken along the <111> zone axis, proved that the top and bottom facets of the hexagonal platelets are the (111) atomic planes. Nonetheless, the as-milled Al–Li-GNSs synthesized in this study showed a hexagonal 2D nanoplatelet morphology rather than a tetrahedral or an octahedral shape. This is directly attributed to the presence of planar defects such as stacking faults and twinning planes which cause deviations from the Gibbs-Wulff equilibrium shape and induce the formation of flat planar nanoparticles [71]. The shape and orientation of the nanoparticles are dictated by the underlying symmetries of the crystals, and internal defect structure such as twinning or stacking faults causes breaking of the regular FCC stacking sequence [59], influencing a 2D growth [60]. Hexagonal and other 2D flat nanoplatelets have been widely observed for FCC metals with low stacking fault energy such as Au and Ag [39–43] and the effect of twinning on the final morphology has been modeled and studied [39,72]. It has been confirmed that hexagonal platelet-like particles with a high aspect ratio form if

multiple parallel twin planes and/or stacking faults exist [39]. Structural and planar defects can occur with high probability during milling due to the high impact energy exerted during the process. Thus, although deformation by twinning in Al is rarely reported due to its relatively high stacking fault energy [48], the formation of twins in nanocrystalline Al synthesized by ball-milling has been reported experimentally [62,73]. Most importantly, recent DFT calculations suggested that alloying Al with Li can reduce the stacking fault energy and activate the formation of twins in nanocrystalline Al [34], which had been observed experimentally [48].

In this context, the presence of forbidden reflections has long been reported for flat thin nanoplatelets and justified by the symmetry breaking in the FCC sequence induced by the presence of planar defects [59]. Others elaborated that the presence of stacking faults and twinning planes in an FCC stacking sequence give rise to the presence of an HCP stacking sequence or HCP domains/layers inside the FCC nanoplatelet [42,59,74]. These HCP domains have been observed microscopically in metallic nanoplatelets and have been suggested to drive the 2D lateral growth of the hexagonal morphology [74]. These conclusions agree with the observations made in this study and take us back to the presence of HCP graphene sheets inside the Al nanoplatelets, and their role in initiating the 2D lateral growth. Based on these observations, we believe that there existed an epitaxial relationship between the Al–Li and GNSs that led to the formation and growth of these hexagonal nanoplatelets.

Thus far, the synthesis of anisotropic metal nanoparticles has been mainly dominated by colloidal/chemical synthesis techniques, where the shape and size of these particles have been controlled chemically by varying the reaction components [1]. It is crucial to study the effect of different milling parameters such as milling time, milling temperature, and ball-to-powder ratio on the final size and morphology of the synthesized nanoplatelets. The non-hexagonal triangle-like Al-based nanoparticles that appear in the SEM images in Fig. 2 around the hexagonal nanoplatelets could be representing a transition state of the Al particles growing into the hexagonal state. Investigating the effect of the milling time on the formation and growth of the anisotropic nanoplatelets is crucial to trace the formation mechanism and the on-set of single-crystal growth. In addition, if the GNSs are acting as substrates providing the building blocks for the formation of these nanoplatelets, changing the graphene content must have severe effects on the size, shape, and yield of these nanoplatelets. Finally, significant efforts have been made in the synthesis of anisotropic metallic nanoparticles with intriguing and novel morphologies using colloidal chemical techniques, yet controversy still persists around the exact nucleation and growth mechanisms of such nanoparticles. Single-crystal growth via a purely mechanical technique and without the use of any additional chemicals, as presented in this study, could change the way the growth of these structures is treated and understood. Introducing the results of this study to the research community is the first step to adopt other perspectives on the reported phenomenon, to encourage further exploration in this field, and to seek proper understanding of the involved formation mechanisms.

5. Conclusion

This study represents the first report of the synthesis of plasmonic single-crystal Al–Li-GNSs with a well-defined hexagonal platelet-like morphology using a simple dry ball-milling technique. It is believed that the interaction at the interface between aluminum and graphene under milling conditions initiated the anisotropic growth, while the presence of Li activated deformation twins and stacking faults which are known to facilitate a well-defined hexagonal nanoplatelet morphology. Understanding the growth of Al on graphene must begin on a 2D scale, yet experimental studies reporting the growth of Al on graphene substrates, to our knowledge, do not exist. The Al system is perhaps one of the simplest to study and the understanding of its interaction with graphene will allow it to be extended to other systems. We only hope to shed light on a new phenomenon and its hidden possibilities in the field of metal/graphene systems and anisotropic metal nanoparticles. We believe the results of this study will lead to new research questions in an aim to further the understanding of the interactions between metals and graphene at their interface, and the role of ball-milling as an integrated top-down/bottom-up synthesis technique. In addition, the reported observations are expected to start a fresh chapter in the fabrication of plasmonic anisotropic metallic nanoparticles for cutting edge-applications.

CRediT authorship contribution statement

Sara I. Ahmad: Conceptualization, Data curation, Formal analysis, Investigation, Methodology, Validation, Visualization, Writing – original draft. **Hicham Hamoudi:** Project administration, Supervision. **Janarthanan Ponraj:** Resources, Investigation. **Khaled M. Youssef:** Conceptualization, Methodology, Funding acquisition, Project administration, Supervision, Writing – review & editing.

Declaration of competing interest

The authors declare that they have no known competing financial interests or personal relationships that could have appeared to influence the work reported in this paper.

Acknowledgment

This work was made possible by NPRP Grant no. NPRP9-180-2-094 from the Qatar National Research Fund (a member of the Qatar Foundation). The statements made herein are solely the responsibility of the authors. The authors would like to acknowledge the technical support provided by Qatar Environment and Energy Research Institute, part of Hamad Bin Khalifa University, and the Central Laboratory Unit and the Center of Advanced Materials at Qatar University.

References

[1] Y. Chen, Z. Fan, Z. Zhang, W. Niu, C. Li, N. Yang, B. Chen, H. Zhang, Two-dimensional metal nanomaterials: synthesis, properties, and applications, Chem. Rev. 118 (2018) 6409.
[2] L. Bu, N. Zhang, S. Guo, X. Zhang, J. Li, J. Yao, T. Wu, G. Lu, J.-Y. Ma, D. Su, X. Huang, Biaxially strained PtPb/Pt core/shell nanoplate boosts oxygen reduction catalysis, Science 354 (2016) 1410.
[3] X. Huang, S. Tang, X. Mu, Y. Dai, G. Chen, Z. Zhou, F. Ruan, Z. Yang, N. Zheng, Freestanding palladium nanosheets with plasmonic and catalytic properties, Nat. Nanotechnol. 6 (2011) 28.
[4] S.R. Beeram, F.P. Zamborini, Selective attachment of antibodies to the edges of gold nanostructures for enhanced localized surface plasmon resonance biosensing, J. Am. Chem. Soc. 131 (2009) 11689.
[5] C. Gao, Z. Lu, Y. Liu, Q. Zhang, M. Chi, Q. Cheng, Y. Yin, Highly stable silver nanoplates for surface plasmon resonance biosensing, Angew. Chem. Int. Ed. 51 (2012) 5629.
[6] B.D. Clark, C.R. Jacobson, M. Lou, D. Renard, G. Wu, L. Bursi, A.S. Ali, D.F. Swearer, A.-L. Tsai, P. Nordlander, N.J. Halas, Aluminum nanocubes have sharp corners, ACS Nano 13 (2019) 9682.
[7] C.R. Jacobson, D. Solti, D. Renard, L. Yuan, M. Lou, N.J. Halas, Shining light on aluminum nanoparticle synthesis, Acc. Chem. Res. 53 (2020) 2020.
[8] P.W. Cooper, Explosives Engineering, John Wiley & Sons, 1996.
[9] Y. Tang, C. Kong, Y. Zong, S. Li, J. Zhuo, Q. Yao, Combustion of aluminum nanoparticle agglomerates: from mild oxidation to microexplosion, Proc. Combust. Inst. 36 (2017) 2325.
[10] C.E. Bunker, M.J. Smith, K.A.S. Fernando, B.A. Harruff, W.K. Lewis, J.R. Gord, E.A. Guliants, D.K. Phelps, Spontaneous hydrogen generation from organic-capped Al nanoparticles and water, ACS Appl. Mater. Interfaces 2 (2010) 11.

[11] P.J. Roach, W.H. Woodward, A.W. Castleman, A.C. Reber, S.N. Khanna, Complementary active sites cause size-selective reactivity of aluminum cluster Anions with water, Science 323 (2009) 492.
[12] J. Kalman, D.K. Smith, K.K. Miller, S.K. Bhattacharia, K.R. Bratton, M.L. Pantoya, A strategy for increasing the energy release rate of aluminum by replacing the alumina passivation shell with aluminum iodate hexahydrate (AlH), Combust. Flame 205 (2019) 327.
[13] G.A. Elia, K. Marquardt, K. Hoeppner, S. Fantini, R. Lin, E. Knipping, W. Peters, J.-F. Drillet, S. Passerini, R. Hahn, An overview and future perspectives of aluminum batteries, Adv. Mater. 28 (2016) 7564.
[14] M.W. Knight, N.S. King, L. Liu, H.O. Everitt, P. Nordlander, N.J. Halas, Aluminum for plasmonics, ACS Nano 8 (2014) 834.
[15] D. Peckus, J. Henzie, T. Tamulevičius, M. Andrulevičius, A. Lazauskas, E. Rajackaitė, Š. Meškinis, S. Tamulevičius, Ultrafast relaxation dynamics of aluminum nanoparticles in solution, Physica E Low Dimens. Syst. Nanostruct. 117 (2020) 113795.
[16] Y. Ekinci, H.H. Solak, J.F. Löffler, Plasmon resonances of aluminum nanoparticles and nanorods, J. Appl. Phys. 104 (2008), 083107.
[17] S.R. Ghanta, K. Muralidharan, Chemical synthesis of aluminum nanoparticles, J. Nanoparticle Res. 15 (2013) 1715.
[18] J.A. Haber, W.E. Buhro, Kinetic instability of nanocrystalline aluminum prepared by chemical synthesis; facile room-temperature grain growth, J. Am. Chem. Soc. 120 (1998) 10847.
[19] M.J. McClain, A.E. Schlather, E. Ringe, N.S. King, L. Liu, A. Manjavacas, M.W. Knight, I. Kumar, K.H. Whitmire, H.O. Everitt, P. Nordlander, N.J. Halas, Aluminum nanocrystals, Nano Lett. 15 (2015) 2751.
[20] K. Park, D. Lee, A. Rai, D. Mukherjee, M.R. Zachariah, Size-resolved kinetic measurements of aluminum nanoparticle oxidation with single particle mass spectrometry, J. Phys. Chem. B 109 (2005) 7290.
[21] M.W. Knight, L. Liu, Y. Wang, L. Brown, S. Mukherjee, N.S. King, H.O. Everitt, P. Nordlander, N.J. Halas, Aluminum plasmonic Nanoantennas, Nano Lett. 12 (2012) 6000.
[22] A. Baladi, R. Sarraf Mamoory, Investigation of different liquid media and ablation times on pulsed laser ablation synthesis of aluminum nanoparticles, Appl. Surf. Sci. 256 (2010) 7559.
[23] M. Yang, Y. Liu, T. Fan, D. Zhang, Metal-graphene interfaces in epitaxial and bulk systems: a review, Prog. Mater. Sci. 110 (2020) 100652.
[24] X. Liu, Y. Han, J.W. Evans, A.K. Engstfeld, R.J. Behm, M.C. Tringides, M. Hupalo, H.-Q. Lin, L. Huang, K.-M. Ho, D. Appy, P.A. Thiel, C.-Z. Wang, Growth morphology and properties of metals on graphene, Prog. Surf. Sci. 90 (2015) 397.
[25] S.I. Ahmad, H. Hamoudi, A. Abdala, Z.K. Ghouri, K.M. Youssef, Graphene-reinforced bulk metal matrix composites: synthesis, microstructure, and properties, Rev. Adv. Mater. Sci. 59 (2020) 67.
[26] K.S. Reddy, D. Sreedhar, K.D. Kumar, G.P. Kumar, Role of reduced graphene oxide on mechanical-thermal properties of aluminum metal matrix nano composites, Mater. Today: SAVE Proc. 2 (2015) 1270.
[27] A. El-Ghazaly, G. Anis, H.G. Salem, Effect of graphene addition on the mechanical and tribological behavior of nanostructured AA2124 self-lubricating metal matrix composite, Compos. Part A Appl. Sci. Manuf. 95 (2017) 325.
[28] H. Yue, L. Yao, X. Gao, S. Zhang, E. Guo, H. Zhang, X. Lin, B. Wang, Effect of ball-milling and graphene contents on the mechanical properties and fracture mechanisms of graphene nanosheets reinforced copper matrix composites, J. Alloys Compd. 691 (2017) 755.
[29] M. Rashad, F. Pan, J. Zhang, M. Asif, Use of high energy ball milling to study the role of graphene nanoplatelets and carbon nanotubes reinforced magnesium alloy, J. Alloys Compd. 646 (2015) 223.
[30] Z. Yu, W. Yang, C. Zhou, N. Zhang, Z. Chao, H. liu, Y. Cao, Y. Sun, P. Shao, G. Wu, Effect of ball milling time on graphene nanosheets reinforced Al6063 composite fabricated by pressure infiltration method, Carbon 141 (2019) 25.
[31] M. Tabandeh-Khorshid, E. Omrani, P.L. Menezes, P.K. Rohatgi, Tribological performance of self-lubricating aluminum matrix nanocomposites: role of graphene nanoplatelets, Eng. Sci. Technol. an Int. 19 (2016) 463.
[32] J.L. Li, Y.C. Xiong, X.D. Wang, S.J. Yan, C. Yang, W.W. He, J.Z. Chen, S.Q. Wang, X.Y. Zhang, S.L. Dai, Microstructure and tensile properties of bulk nanostructured aluminum/graphene composites prepared via cryomilling, Mater. Sci. Eng. 626 (2015) 400.
[33] R. Pérez-Bustamante, D. Bolaños-Morales, J. Bonilla-Martínez, I. Estrada-Guel, R. Martínez-Sánchez, Microstructural and hardness behavior of graphene-nanoplatelets/aluminum composites synthesized by mechanical alloying, J. Alloys Compd. 615 (2014) S578.
[34] M. Muzyk, Z. Pakieła, K.J. Kurzydłowski, Generalized stacking fault energies of aluminum alloys—density functional theory calculations, Metals 8 (2018) 823.
[35] I.J. Polmear, Aluminium alloys — a century of age hardening, Mater. Forum 28 (2004) 1.
[36] Y. Jiang, Z. Tan, R. Xu, G. Fan, D.-B. Xiong, Q. Guo, Y. Su, Z. Li, D. Zhang, Tailoring the structure and mechanical properties of graphene nanosheet/aluminum composites by flake powder metallurgy via shift-speed ball milling, Compos. Part A Appl. Sci. Manuf. 111 (2018) 73.
[37] M. Samadi Khoshkhoo, S. Scudino, T. Gemming, J. Thomas, J. Freudenberger, M. Zehetbauer, C.C. Koch, J. Eckert, Nanostructure formation mechanism during in-situ consolidation of copper by room-temperature ball milling, Mater. Des. 65 (2015) 1083.
[38] S.E. Shin, H.J. Choi, J.H. Shin, D.H. Bae, Strengthening behavior of few-layered graphene/aluminum composites, Carbon 82 (2015) 143.
[39] D.L. Lyutov, K.V. Genkov, A.D. Zyapkov, G.G. Tsutsumanova, A.N. Tzonev, L.G. Lyutov, S.C. Russev, Synthesis and structure of large single crystalline silver hexagonal microplates suitable for micromachining, Mater. Chem. Phys. 143 (2014) 642.
[40] V. Germain, J. Li, D. Ingert, Z.L. Wang, M.P. Pileni, Stacking faults in formation of silver nanodisks, J. Phys. Chem. B 107 (2003) 8717.
[41] Y. Yang, S. Matsubara, L. Xiong, T. Hayakawa, M. Nogami, Solvothermal synthesis of multiple shapes of silver nanoparticles and their SERS properties, J. Phys. Chem. C 111 (2007) 9095.
[42] M.C. Mendoza-Ramirez, H.G. Silva-Pereyra, M. Avalos-Borja, Hexagonal phase into Au plate-like particles: a precession electron diffraction study, Mater. Char. 164 (2020) 110313.
[43] Y. Chen, X. Gu, C.-G. Nie, Z.-Y. Jiang, Z.-X. Xie, C.-J. Lin, Shape controlled growth of gold nanoparticles by a solution synthesis, Chem. Commun. (J. Chem. Soc. Sect. D) (2005) 4181.
[44] B.D. Clark, C.R. Jacobson, M. Lou, J. Yang, L. Zhou, S. Gottheim, C.J. DeSantis, P. Nordlander, N.J. Halas, Aluminum nanorods, Nano Lett. 18 (2018) 1234.
[45] K.J. Smith, Y. Cheng, E.S. Arinze, N.E. Kim, A.E. Bragg, S.M. Thon, Dynamics of energy transfer in large plasmonic aluminum nanoparticles, ACS Photonics 5 (2018) 805.
[46] H. Yu, P. Zhang, S. Lu, S. Yang, F. Peng, W.-S. Chang, K. Liu, Synthesis and multipole plasmon resonances of spherical aluminum nanoparticles, J. Phys. Chem. Lett. 11 (2020) 5836.
[47] K.M. Youssef, R.O. Scattergood, K.L. Murty, C.C. Koch, Nanocrystalline Al–Mg alloy with ultrahigh strength and good ductility, Scripta Mater. 54 (2006) 251.
[48] S.I. Ahmad, L.A. Al-Sulaiti, K.A. Mkhoyan, K.M. Youssef, Artifact-free bulk nanocrystalline Al-Li alloys with multiple deformation mechanisms and improved tensile properties, Mater, Today Commun 25 (2020) 101607.
[49] S.J. Huang, A. Muneeb, A. Abbas, R. Sankar, The effect of Mg content and milling time on the solid solubility and microstructure of Ti–Mg alloys processed by mechanical milling, J. Mater. Res. Technol. 11 (2021) 1424.
[50] H.X. Sui, M. Zhu, M. Qi, G.B. Li, D.Z. Yang, The enhancement of solid solubility limits of AlCo intermetallic compound by high-energy ball milling, J. Appl. Phys. 71 (1992) 2945.
[51] A. Bhadauria, L.K. Singh, T. Laha, Combined strengthening effect of nanocrystalline matrix and graphene nanoplatelet reinforcement on the mechanical properties of spark plasma sintered aluminum based nanocomposites, Mater. Sci. Eng. 749 (2019) 14.
[52] A.C. Ferrari, J.C. Meyer, V. Scardaci, C. Casiraghi, M. Lazzeri, F. Mauri, S. Piscanec, D. Jiang, K.S. Novoselov, S. Roth, A.K. Geim, Raman spectrum of graphene and graphene layers, Phys. Rev. Lett. 97 (2006) 187401.
[53] N.T. Aboulkhair, M. Simonelli, E. Salama, G.A. Rance, N.C. Neate, C.J. Tuck, A.M.K. Esawi, R.J.M. Hague, Evolution of carbon nanotubes and their metallurgical reactions in Al-based composites in response to laser irradiation during selective laser melting, Mater. Sci. Eng. 765 (2019) 138307.
[54] M. Bastwros, G.-Y. Kim, C. Zhu, K. Zhang, S. Wang, X. Tang, X. Wang, Effect of ball milling on graphene reinforced Al6061 composite fabricated by semi-solid sintering, Compos. B Eng. 60 (2014) 111.
[55] S.H. Huh, Thermal reduction of graphene oxide, in: S. Mikhailov (Ed.), Physics and Applications of Graphene-Experiments, InTech, 2011, pp. 73–90.
[56] L. Yuan, C. Zhang, X. Zhang, M. Lou, F. Ye, C.R. Jacobson, L. Dong, L. Zhou, M. Lou, Z. Cheng, Photocatalytic hydrogenation of graphene using Pd nanocones, Nano Lett. 19 (2019) 4413.
[57] L. Yuan, M. Lou, B.D. Clark, M. Lou, L. Zhou, S. Tian, C.R. Jacobson, P. Nordlander, N.J. Halas, Morphology-dependent reactivity of a plasmonic photocatalyst, ACS Nano 14 (2020) 12054.
[58] J.C. Heyraud, J.J. Métois, Anomalous 13 422 diffraction spots from {111} flat gold crystallites: (111) surface reconstruction and moiré fringes between the surface and the bulk, Surf. Sci. 100 (1980) 519.
[59] M.K. Singh, B. Mukherjee, R.K. Mandal, Growth morphology and special diffraction characteristics of multifaceted gold nanoparticles, Micron 94 (2017) 46.
[60] B. Viswanath, P. Kundu, B. Mukherjee, N. Ravishankar, Predicting the growth of two-dimensional nanostructures, Nanotechnology 19 (2008) 195603.
[61] F. Kemper, E. Beckert, R. Eberhardt, A. Tuennermann, Light filter tailoring the impact of light emitting diode irradiation on the morphology and optical properties of silver nanoparticles within polyethylenimine thin films, RSC Adv. 7 (2017) 41603.
[62] S.I. Ahmed, K.A. Mkhoyan, K.M. Youssef, The activation of deformation mechanisms for improved tensile properties in nanocrystalline aluminum, Mater. Sci. Eng. 777 (2020) 139069.
[63] X. Shang, X. Wang, S. Chen, Effects of ball milling processing conditions and alloy components on the synthesis of Cu-Nb and Cu-Mo alloys, Materials 12 (2019).
[64] M. Ramezani, T. Neitzert, Mechanical milling of aluminum powder using planetary ball milling process, J. Achiev. Mater. Manuf. Eng. 55 (2012) 790.
[65] B. Xiong, K. Liu, Q. Yan, W. Xiong, X. Wu, Microstructure and mechanical properties of graphene nanoplatelets reinforced Al matrix composites fabricated by spark plasma sintering, J. Alloys Compd. 837 (2020) 155495.
[66] B. Guo, B. Chen, X. Zhang, X. Cen, X. Wang, M. Song, S. Ni, J. Yi, T. Shen, Y. Du, Exploring the size effects of Al4C3 on the mechanical properties and thermal behaviors of Al-based composites reinforced by SiC and carbon nanotubes, Carbon 135 (2018) 224.
[67] X. Liu, C.-Z. Wang, M. Hupalo, H.-Q. Lin, K.-M. Ho, M.C. Tringides, Metals on graphene: interactions, growth morphology, and thermal stability, Crystals 3

(2013) 40007.
[68] A.Y. Galashev, O.R. Rakhmanova, Computational study of the formation of aluminum-graphene nanocrystallites, Phys. Lett. 384 (2020) 126790.
[69] S. Kumar, Graphene Engendered aluminium crystal growth and mechanical properties of its composite: an atomistic investigation, Mater. Chem. Phys. 208 (2018) 41.
[70] G.D. Barmparis, Z. Lodziana, N. Lopez, I.N. Remediakis, Nanoparticle shapes by using Wulff constructions and first-principles calculations, Beilstein J. Nanotechnol. 6 (2015) 361.
[71] T.K. Sau, A.L. Rogach, Nonspherical noble metal nanoparticles: colloid-chemical synthesis and morphology control, Adv. Mater. 22 (2010) 1781.
[72] C.B. Murray, S. Sun, H. Doyle, T. Betley, Monodisperse 3d transition-metal (Co, Ni, Fe) nanoparticles and their assembly into nanoparticle superlattices, MRS Bull. 26 (2001) 985.
[73] X. Liao, F. Zhou, E. Lavernia, S. Srinivasan, M. Baskes, D. He, Y. Zhu, Deformation mechanism in nanocrystalline Al: partial dislocation slip, Appl. Phys. Lett. 83 (2003) 632.
[74] D. Aherne, D.M. Ledwith, M. Gara, J.M. Kelly, Optical properties and growth aspects of silver nanoprisms produced by a highly reproducible and rapid synthesis at room temperature, Adv. Funct. Mater. 18 (2008) 2005.